IMPROVEMENT OF CAPTURE RATIO FOR AN X-BAND LINAC BASED ON MULTI-OBJECTIVE GENETIC ALGORITHM*

Junyang Li, Tongning Hu†, Jun Yang, Bingqian Zeng, Hongjie Xu, Lanxin Nie
Huazhong University of Science and Technology, Wuhan, China

Abstract

Electron linear accelerators with an energy of ~MeV are widely required in industrial applications. Whereas miniaturized accelerators, especially those working at X-band, attract more and more attention due to their compact structures and high gradients. Since the performance of a traveling wave (TW) accelerator is determined by its structures, considerable efforts must be made for structure optimization involving numerous and complex parameters. In this context, functional key parameters are obtained through deep analysis for structure and particle motion characteristics of the TW accelerator, then a multi-objective genetic algorithm (MOGA) is successfully applied to acquire an optimized phase velocity distribution which can contribute to achieving a high capture ratio and a low energy spread. Finally, a low-energy X-band TW tube used for rubber vulcanization is taken as an example to verify the reliability of the algorithm under a single-particle model. The capture ratio is 91.2%, while the energy spread is 5.19%, and the average energy is 3.1MeV.

INTRODUCTION

Electron beams with energy of ~MeV have been widely applied in life and materials sciences, industrial radiography, wastewater treatment, non-destructive testing, and other fields [1-4]. In recent years, Chiang Mai University in Thailand has researched applying electron beam of ~MeV to rubber vulcanization. The research on vulcanization of rubber was carried out by Chiang Mai University in Thailand Considering the difference in material thickness and density, the beam energy is generally 1-4 MeV [5-7].

RF linac is a commonly used scheme to obtain electron beam of ~MeV, but the traditional S-band accelerator structure and supporting power sources are relatively large, which is not suitable for cargo inspection and other occasions requiring accelerator miniaturization [8]. In contrast, the X-band increases the operating frequency by about three times, which has the advantages of a high acceleration gradient and compact structure. At present, many accelerator laboratories have developed X-band accelerators [9-13].

In the design of phase velocity for the TW tubes, it is often necessary to try repeatedly according to engineering experience, which is time-consuming and difficult to gain the optimal performance parameters. In 2002 Deb proposed nondominated sorting genetic algorithm II (NSGA-II), which has good convergence and diversity in solving multi-objective problems [14]. Based on NSGA-II, many

___

† TongningHu@hust.edu.cn

accelerator-related optimization problems have been completed, such as beam matching and beam transport in the low and medium energy section of a modern hadron linac [15], undulator taper profile and focusing scheme of a seeded free electron laser (FEL) [16], the optimal working point of a linac driver for a seeded FEL [17], the nonlinear lattice and dynamic aperture for the high energy photon source storage ring [18,19].

In consequence, it is of engineering significance to optimize the phase velocity of low-energy X-band TW tubes by using the multi-objective genetic algorithm. After introducing the mathematical and physical model of TW acceleration structure, NSGA-II is used to obtain the Pareto front with the goal of high capture ratio and low energy spread. At last, one of the points in the Pareto front is selected to analyze single-particle motion.

DESIGN CONSIDERATIONS OF X-BAND LINAC

As mentioned in the last section, MOGA is a good choice for optimizing the TW tubes. For sake of applying the algorithm better, it is necessary to convert physics problems into mathematics problems reasonably.

Basic Theory

Designing the TW tubes with the iris-loaded waveguide structure requires the relationships between the field strength E and the power P, as a consequence of beam loading effect must be considered in actual operation，the relationships should be expressed as follows.

$$E(z) = \sqrt{2\alpha Z_s P(z)} \tag{1}$$

$$\frac{dP(z)}{dz} = -2\alpha P(z) - IE(z) \tag{2}$$

where α is the attenuation factor, Z_s is the shunt impedance, z is the longitudinal position in the TW tubes, and I is the average beam current.

As for Eq. (1) and (2), P is given at the beginning of the design, α and Z_s are determined by designing the structure according to the target field strength. α could be directly obtained by the two-dimensional electromagnetic field software SUPERFISH, while Z_s could be calculated by the group velocity v_g, the quality factor Q, and the angular frequency ω, stated as the following.

$$\alpha = \frac{\omega}{2 v_g Q} \tag{3}$$

The above-mentioned field strength distribution should be designed according to the quality requirements of the

output particles. The longitudinal motion of particles under the field strength is shown as:

$$\frac{d\gamma}{dz} = -\frac{eE}{m_0 c^2}\sin\varphi \tag{4}$$

$$\frac{d\varphi}{dz} = \frac{2\pi}{\lambda}\left(\frac{1}{\beta_p} - \frac{\gamma}{\sqrt{\gamma^2 - 1}}\right) \tag{5}$$

where γ is the relativistic mass factor, φ is the phase, e is the electron charge, $m_0 c^2$ is the rest energy of the electron, λ is the radio frequency wavelength, and β_p is the cavity phase velocity.

Preparations for Optimizing Design

As introduced in the last subsection, α and Z_s are calculated by SUPERFISH, while different β_p have different α and Z_s. The following Fig. 1 shows the 1.5 cell model at $\beta_p = 0.50$ in SUPERFISH and the corresponding single-cavity three-dimensional model.
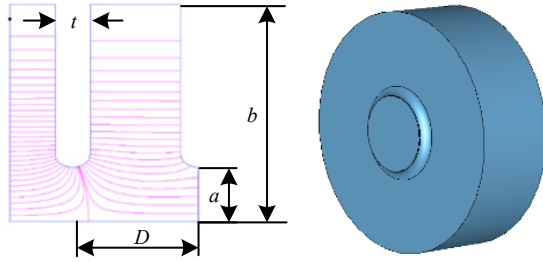

Figure 1: $\beta_p = 0.50$ (a) 1.5 cell two-dimensional model, (b) three-dimensional model of single-cavity, where D is the cavity length, a is the iris radius, b is the waveguide radius, and t is the iris thickness.

As we known, the low-energy linac needs to rely on the variable β_p to achieve particle capture, so the front end of the TW tubes has a wide variation. Thus, a reasonable design will be considered about the distribution of β_p in the cavity chain to obtain a higher capture ratio. The application of the MOGA can improve the design efficiency, but the relationship between the parameters needs to be established in advance, especially the changes of α and Z_s with β_p.

Taking the initial power of 1 MW and the initial beam energy of 45keV as an example, to achieve an acceleration of about 3MeV and a high capture ratio, firstly calculate the field strength according to Eq. (1) and Eq. (2) for each cavity, then exit energy and phase could be obtained according to Eq. (4) and Eq. (5), which determines capture ratio and energy spread. As the key parameters, the calculations for α and Z_s are time-consuming and inconvenient because SUPERFISH must be re-called cell by cell in the programming. The range of β_p is selected as [0.35,1.11] due to the initial energy of the electrons and several points of α and Z_s are chose to fit. To improve

efficiency, the variation of α with β_p is expressed by Gaussian fitting and the variation of Z_s with β_p is expressed by polynomial fitting. The expressions are written as.

$$\alpha = 25510\exp\left(-\left(\frac{\beta_p + 0.8152}{0.3694}\right)^2\right)$$
$$+ 18.73\exp\left(-\left(\frac{\beta_p + 0.5809}{0.6113}\right)^2\right) \tag{6}$$
$$+ 1.888\exp\left(-\left(\frac{\beta_p + 0.8879}{2.733}\right)^2\right)$$

$$Z_s = -132.05\beta_p{}^5 + 657.31\beta_p{}^4$$
$$-1320.5\beta_p{}^3 + 1292.7\beta_p{}^2 - 434.43\beta_p + 47.908 \tag{7}$$

Corresponding fitting curves of α and Z_s are displayed in Fig. 2. Obviously, the fitting curves are consistent with the calculation results of SUPERFISH well. The sum of squares due to error (SSE) of the attenuation factor is 9.3391×10^{-5} and coefficient of determination R-square is 1, SSE of the shunt impedance is 0.0046 and R-square is also 1. Since the closer R-square is to 1, the better the data fit, it is feasible to solve α and Z_s by fitting functions.
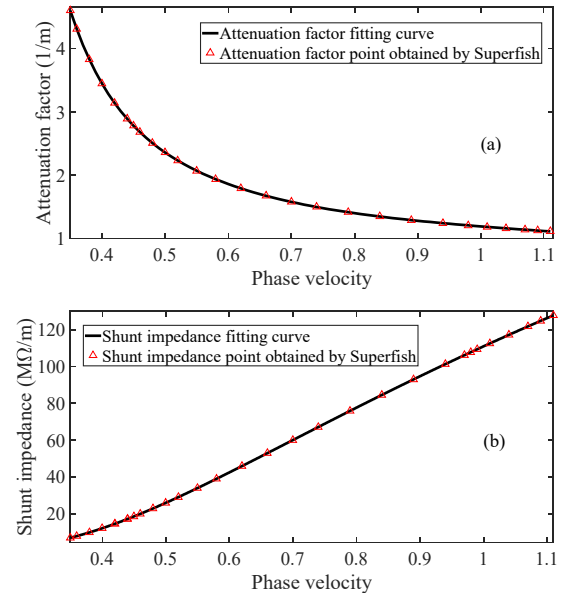

Figure 2: Fitting at different phase velocities (a) attenuation factor, (b) shunt impedance.

Note that, to simplify the structure design and realization, the same iris radius is used here. Combining previous literature and engineering experiences [20], the structure of the six-segment cavity chain is adopted. As the energy of the electron is lower, the increment of the electron phase velocity $\Delta\beta_e$ to a certain energy increase is larger, so it is reasonable that the number of cavities in each segment gradually increases while the corresponding variable range of β_p gradually decreases. The initial energy of the electron

is 45 keV, and the corresponding electron phase velocity β_e is 0.394. Let the variable range of the first segment β_p is around 0.394, then gradually increase the value of each segment β_p. Finally, the range of β_p and the number of cells for the six segments are shown in the table below.

Table 1: The Range of β_p and the Number of Cells for the Six Segments

	1	2	3	4	5	6
$\beta_{p\min}$	0.36	0.50	0.72	0.92	0.96	0.98
$\beta_{p\max}$	0.43	0.57	0.75	0.95	0.97	0.99
Number of cells	4	5	5	6	6	16

SIMULATIONS BASED ON MOGA

To verify the optimizing scheme, NSGA-II is applied to chase phase velocity distribution in this section.

MOGA Combined with the TW Tubes

In the cases of multi-objective X-band TW tubes, β_p of each cavity is chosen as the variable, while the capture ratio η and the energy spread σ are set as the goals. η and σ are determined by the energy and phase at the exit of the linac.

The electrons that can be stably accelerated in the TW tubes are called captured electrons. The expression of η is as follows:

$$\eta=\frac{M}{N}\times100\% \tag{8}$$

where N is the initial number of electrons whose entrance phase is uniformly distributed in $\left[-360^{\circ},0\right]$. Suppose φ_1 is the median phase of these N electrons at the last cell, and M is the number of electrons whose phase at the exit is $\left[\varphi_1-180^{\circ},\varphi_1+180^{\circ}\right]$. In this context, N is set to 500, so that the accuracy of the capture ratio is 0.2%.

Since the program obtains M energy points, it is more convenient to measure energy spread in the form of root mean square. The expression of σ is as follows:

$$\sigma=\frac{1}{\overline{W}}\sqrt{\frac{1}{M}\sum_{i=1}^{M}\left(W_i-\overline{W}\right)^2} \tag{9}$$

where W_i is the exit energy of different initial phases, and $\overline{W}$ is the average energy. Both W_i and $\overline{W}$ are for the captured particles.

The optimization process of the TW tubes structure is shown in Fig. 3. First, 200 population individuals with different β_p are initialized, and then the fitness function values of individuals in the population are calculated and fast non-dominated sorting is performed. The individuals with a small non-dominated serial number are selected through

the tournament. If the serial number is the same, the previous individual will be chosen. After crossover and mutation, the first generation of offspring population is obtained and merged with the parent population. Then calculate the fitness function value for the merged population and get the stratification result after fast non-dominated sorting. After completing the above steps, calculate the crowdedness of the individuals and fill in the individuals with small non-dominated serial numbers and high crowdedness into the new parent population up to 200. Finally, select, crossover and mutation as before to get the offspring population. After 30 generations of cycles, the individuals with the smallest non-dominated serial number are output.
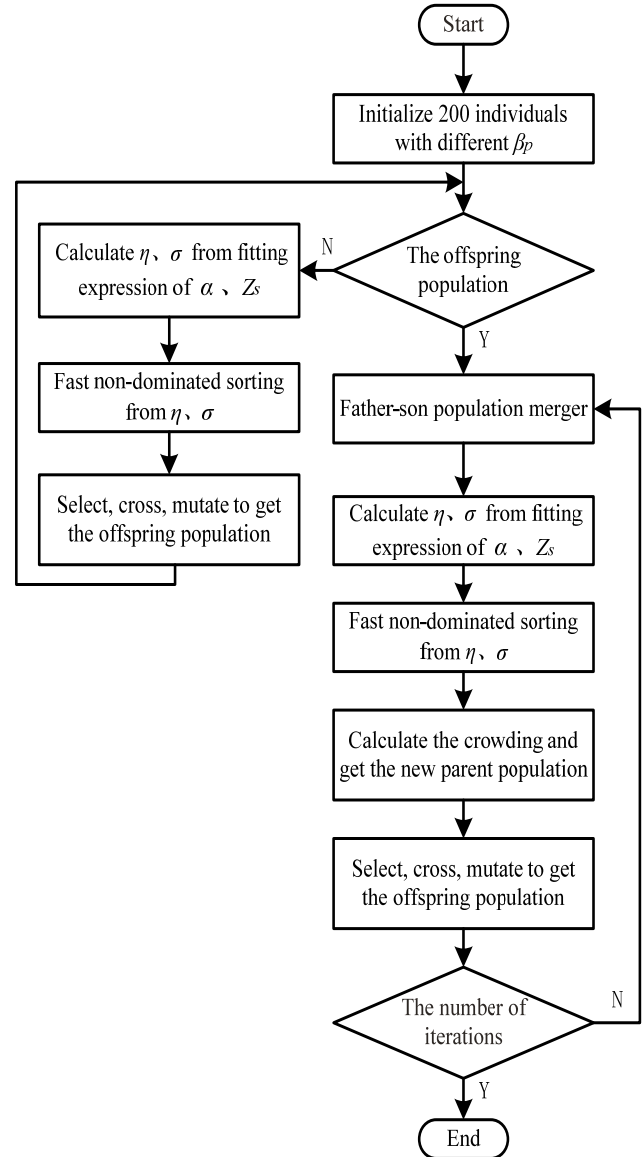

Figure 3: Flow chart of optimizing the TW tubes with NSGA-II.

The eight Pareto front points obtained by using NSGA-II are shown in Fig. 4(a). The corresponding capture ratio ranges from 87.4% to 92.0%, and the energy spread ranges from 4.18% to 5.52%.
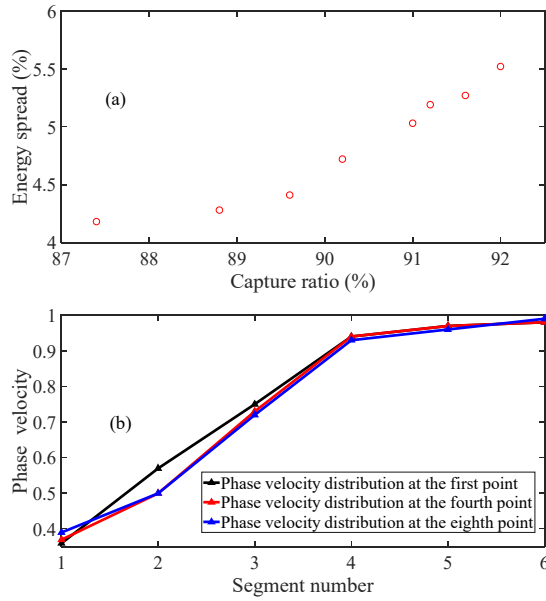
Figure 4: Pareto front and phase velocity distribution.

In Fig. 4(a), take the representative points 1, 4, and 8 from left to right and gain the corresponding phase velocity distribution as shown in Fig. 4(b). It can be seen that the capture ratio and energy spread are related to the first two segments of the cavity chain. The greater the phase velocity of the first segment, the higher the capture ratio and the smaller the energy spread.

Beam Dynamics Based on Single-particle Model

To analyze the movement process of electrons in the TW tubes, the sixth Pareto front point of Fig. 4(a) from left to right is selected. The phase and energy change along with the longitudinal position of the TW tubes are shown in the Fig. 5 below.
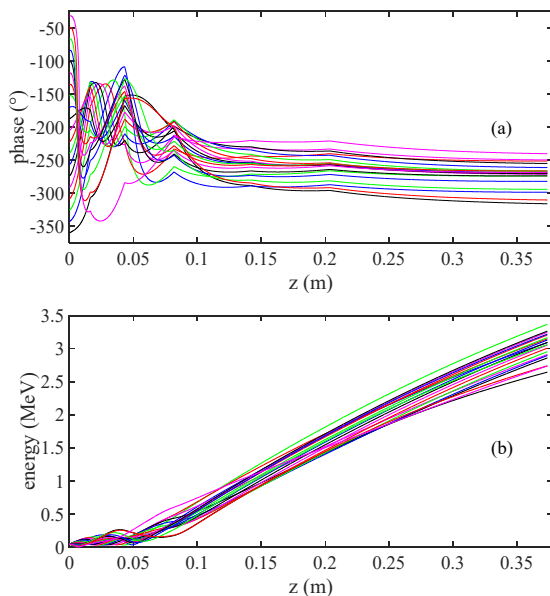

Figure 5: Change along with the longitudinal position z of the TW tubes (a) Phase, (b) Energy.

It can be seen from Figure 5(a) that 328° can be captured with an initial phase width of 360°, and the capture ratio is 91.2%. The captured electrons oscillate in phase in the first half of the cavity chain, and the phase gradually decreases and stabilizes after 0.1m in the longitudinal position. There are non-differentiable points in the phase distribution due to the sudden change of β_p at the segment junction, and its number and position corresponding to the number and position of β_p sudden change. It can be seen from Fig. 5(b) that the energy of the captured electrons oscillates with the phase oscillation in the first half of the cavity chain. Since the phase gradually stabilizes after 0.1m in the longitudinal position, the energy increases approximately linearly.

To analyze the capture ratio and energy spread, the distributions of phase and energy at the exit of the TW tubes are plotted as shown in the Fig. 6 below.
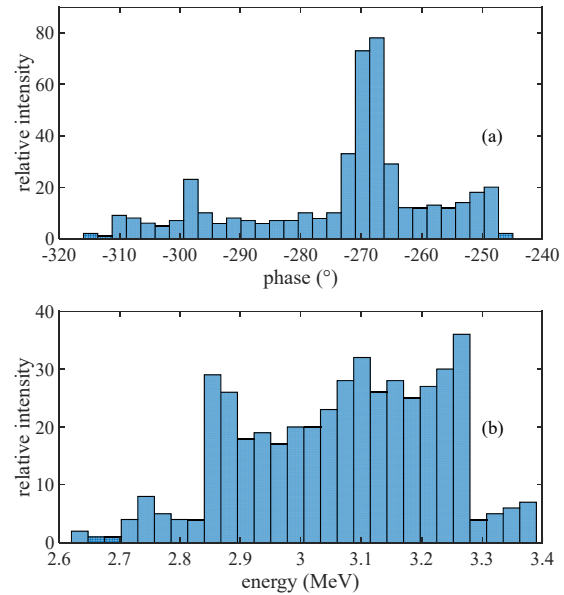

Figure 6: Distribution (a)exit phase, (b)exit energy.

It can be seen from Fig. 6(a) that the exit phase of the captured electrons is compressed to 75°. The exit phase of most electrons is concentrated at the maximum acceleration phase of -270°, so the cavity with β_p of 0.99 can be expanded to increase the exit energy. It can be seen from Fig. 6(b) that the exit energy of the captured electrons is distributed within 2.6~3.4MeV, most of which are concentrated in 2.9~3.3MeV. The average energy is 3.1MeV and the energy spread is 5.19%.

CONCLUSION

For the reasonable application of the MOGA in improving the design efficiency for X-band linac, the fitting of the attenuation factor and the shunt impedance with respect to the phase velocity distribution of the acceleration unit is proposed in the structure of identical iris radius. The coefficient of determination R-square shows that the fitted model is feasible. To simplify the structural design and improve the capture ratio, the form of six segments is adopted and the variable phase velocity range of each section is

given. By establishing a quantitative relationship between capture ratio, energy spread and exit phase, exit energy, the fitness function is linked to the output of the single-particle model. Based on NSGA-II, the phase velocity distribution with high capture ratio and low energy spread is obtained, which provides the design basis for ~MeV TW cube that can be used in the industry. In addition, the algorithm can be extended to the situation where the phase velocity and field strength can be changed cell by cell, resulting in a higher capture ratio and lower energy spread.

REFERENCES

[1] V. M. Tsakanov et al., "AREAL low energy electron beam applications in life and materials sciences," Nuclear Instruments and Methods in Physics Research Section A: Accelerators, Spectrometers, Detectors and Associated Equipment, vol. 829, pp. 248-253, 2016. doi:10.1016/j.nima.2016.02.028

[2] A. J. Antolak, "Overview of Accelerator Applications for Security and Defense," in Reviews of Accelerator Science and Technology: World Scientific, 2016, pp. 27-36. doi:10.1142/9789813108905_0002

[3] S. Machi, "Trends for Electron Beam Accelerator Applications in Industry," Reviews of Accelerator Science and Technology, vol. 04, no. 01, pp. 1-10, 2011. doi:10.1142/S1793626811000562

[4] W. A. Reed, "Nondestructive Testing and Inspection Using Electron Linacs," in Industrial Accelerators and Their Applications: World Scientific, 2011, pp. 307-369. doi:10.1142/9789814307055_0008

[5] P. Apiwattanakul and S. Rimjaem, "Electron beam dynamic study and Monte Carlo simulation of accelerator-based irradiation system for natural rubber vulcanization," Nuclear Instruments and Methods in Physics Research Section B: Beam Interactions with Materials and Atoms, vol. 466, pp. 69-75, 2020. doi:10.1016/j.nimb.2020.01.012

[6] S. Rimjaem, E. Kongmon, M. W. Rhodes, J. Saisut, and C. Thongbai, "Electron linear accelerator system for natural rubber vulcanization," Nuclear Instruments and Methods in Physics Research Section B: Beam Interactions with Materials and Atoms, vol. 406, pp. 233-238, 2017. doi:10.1016/j.nimb.2016.11.016

[7] J. Saisut, M. W. Rhodes, E. Kongmon, S. Rimjeam, and C. Thongbai, "RF System of Linear Accelerator for Natural Rubber Research," Journal of Physics: Conference Series, vol. 1144, p. 012157, 2018. doi:10.1088/1742-6596/1144/1/012157

[8] S. V. Kutsaev, "Novel Technologies for Compact Electron Linear Accelerators (Review)," Instruments and Experimental Techniques, vol. 64, no. 5, pp. 641-656, 2021. doi:10.1134/S0020441221050079

[9] S. V. Kutsaev et al., "Compact X-Band electron linac for radiotherapy and security applications," Radiation Physics and Chemistry, vol. 185, p. 109494, 2021. doi:10.1016/j.radphyschem.2021.109494

[10] J. Shi, A. Grudiev, and W. Wuensch, "Tuning of X-band traveling-wave accelerating structures," Nuclear Instruments and Methods in Physics Research Section A: Accelerators, Spectrometers, Detectors and Associated Equipment, vol. 704, pp. 14-18, 2013. doi:10.1016/j.nima.2012.11.182

[11] G. Gatti et al., "X-band accelerator structures: On going R&D at the INFN," Nuclear Instruments and Methods in Physics Research Section A: Accelerators, Spectrometers, Detectors and Associated Equipment, vol. 829, pp. 206-212, 2016. doi:10.1016/j.nima.2016.02.061

[12] S. Kim et al., "Development of a compact X-band linear accelerator system mounted on an O-arm rotating gantry for radiation therapy," Review of Scientific Instruments, vol. 92, no. 2, p. 024103, 2021. doi:10.1063/5.0030271

[13] X. Huang, W. Fang, Q. Gu, and Z. Zhao, "Design of an X-band accelerating structure using a newly developed structural optimization procedure," Nuclear Instruments and Methods in Physics Research Section A: Accelerators, Spectrometers, Detectors and Associated Equipment, vol. 854, pp. 45-52, 2017. doi:10.1016/j.nima.2017.02.050

[14] K. Deb, A. Pratap, S. Agarwal, and T. Meyarivan, "A fast and elitist multiobjective genetic algorithm: NSGA-II," IEEE Transactions on Evolutionary Computation, vol. 6, no. 2, pp. 182-197, 2002. doi:10.1109/4235.996017

[15] M. Yarmohammadi Satri, A. M. Lombardi, and F. Zimmermann, "Multiobjective genetic algorithm approach to optimize beam matching and beam transport in high-intensity hadron linacs," Physical Review Accelerators and Beams, vol. 22, no. 5, p. 054201, 2019. doi:10.1103/PhysRevAccelBeams.22.054201

[16] J. Wu et al., "Multi-Dimensional Optimization of a Terawatt Seeded Tapered Free Electron Laser with a Multi-Objective Genetic Algorithm," Nuclear Instruments and Methods in Physics Research Section A: Accelerators, Spectrometers, Detectors and Associated Equipment, vol. 846, 2016. doi:10.1016/j.nima.2016.11.035

[17] R. Bartolini, M. Apollonio, and I. P. S. Martin, "Multiobjective genetic algorithm optimization of the beam dynamics in linac drivers for free electron lasers," Physical Review Special Topics - Accelerators and Beams, vol. 15, no. 3, p. 030701, 2012. doi:10.1103/PhysRevSTAB.15.030701

[18] J. Wan, P. Chu, Y. Jiao, and Y. Li, "Improvement of machine learning enhanced genetic algorithm for nonlinear beam dynamics optimization," Nuclear Instruments and Methods in Physics Research Section A Accelerators Spectrometers Detectors and Associated Equipment, p. 162683, 2019. doi:10.1016/j.nima.2019.162683

[19] W. Gao, L. Wang, and W. Li, "Simultaneous optimization of beam emittance and dynamic aperture for electron storage ring using genetic algorithm," Physical Review Special Topics - Accelerators and Beams, vol. 14, no. 9, p. 094001, 2011. doi:10.1103/PhysRevSTAB.14.094001

[20] C. Yao, Electron Linear Accelerator, China: Science Press, 1986.